ZR-CONTAINING LAYERED DOUBLE HYDROXIDES: SYNTHESIS, CHARACTERIZATION, AND EVALUATION OF THERMODYNAMIC PROPERTIES

Poonoosamy J. [1]*, Brandt F. [1], Stekiel M.[2], Kegler P.[1], Klinkenberg M.[1], Winkler B.[2], Vinograd V.[1], Bosbach D.[1], Deissmann G.[1]

[1]Forschungszentrum Jülich GmbH, IEK-6: Institute of Nuclear Waste Management and Reactor Safety, 52425 Jülich, Germany

[2] Goethe Universität Frankfurt, Institute of Geosciences, 60438 Frankfurt, Germany

*corresponding author: j.poonoosamy@fz-juelich.de

Abstract

Layered doubled hydroxides (LDH), consisting of positively charged octahedral brucite-type layers and interlayer anions, have been widely studied in the last decades because of their ability to control the mobility of various anions and cations in the environment. LDH may be relevant to the safety case of nuclear waste repositories due to their retention potential of anionic radionuclide species, for example ^{129}I or ^{79}Se. So far few studies were dedicated to Zr incorporation into LDH, which might be a relevant secondary phase in the repository environment due to the possible corrosion of Zr-bearing nuclear materials and the presence of ^{93}Zr, a long-lived fission and activation product, in various nuclear waste streams. The focus of our study was to synthesize and characterize Cl-bearing Mg-Al-LDH ($Mg_xAl_yZr_z(OH)_2Cl_{(2x+3y+4z-2)}$) with different Zr-content and to evaluate their thermodynamic properties, especially their solubility as a function of temperature. The LDH were synthesized by a coprecipitation method at temperatures between 298.15 and 343.15 K, aiming at Zr/(Zr+Al) ratios of 0.1 and 0.4, respectively. Our analytical techniques combining X-ray diffraction and scanning electron microscopy indicated that up to 5 mol% Zr were incorporated into the brucite

layer of the LDH. At higher Zr concentrations the precipitation of an amorphous hydrous Zr-oxide was observed. The structural uptake of Zr was lower than the value reported in literature for CO_3^{2-} bearing LDH, suggesting that the interlayer anions may play a role with regard to the Zr uptake in the brucite layer. At low Zr contents, well defined crystalline LDH with the composition $Mg_{0.72}Al_{0.22}Zr_{0.025}(OH)_2Cl_{0.20}$ were obtained at all syntheses temperatures. The solubility of this LDH decreases slightly with temperature and the stoichiometric saturation constant was found to satisfy the Van't Hoff equation. The thermodynamic properties of the Zr LDH (Gibbs free energy of formation, ΔG°_f) were determined by considering an approach based on solubility data and Gibbs energy minimization and a calorimetric approach. The enthalpy of formation (ΔH°_f) and the lattice entropy (S°) of the Zr-LDH were determined using calorimetric measurements to be -1181.01±4.98 $kJmol^{-1}$ and 83.9 $Jmol^{-1}K^{-1}$ respectively. Considering contribution of the configurational entropy, the standard entropy, S°, was evaluated at 97±7 $Jmol^{-1}K^{-1}$. The ΔG°_f for $Mg_{0.72}Al_{0.22}Zr_{0.025}(OH)_2Cl_{0.20}*0.69H_2O$ obtained from experimental measurements and that predicted by theory were evaluated at -1046 ± 7 and -1046 ± 13 $kJmol^{-1}$ respectively. Thus, the combination of solubility data and Gibbs energy minimization can be considered as good alternative for the evaluation of ΔG°_f of LDH.

Keywords: ZrMgAl-LDH, solubility, ΔG°_f, S°, ΔH°_f

1 Introduction

Layered double hydroxides (LDH), also known as anionic clays, have intensively been studied during the last decades due to their wide range of industrial applications and their ability to control contaminant mobility in wastes as well as in the environment (Cavani et al., 1991; Scheidegger et al., 1997; Rives, 2001; Johnson and Glasser, 2003; Allada et al., 2005a; Skovbjerg et al., 2010; Mills et al., 2012). The structure of LDH compounds is characterized by layers with a brucite-like structure of octahedrally coordinated divalent cations, forming two-dimensional infinite layers by edge sharing of the octahedra (Ingram and Taylor, 1967; Allmann and Jepsen, 1969; Allmann, 1970; Taylor, 1973; Cavani et al., 1991; Drits and Bookin, 2001; Allada et al., 2005a). The layers carry a net positive charge, usually due to a partial isomorphous substitution of the divalent cations by trivalent (or more rarely tetravalent) cations giving a general layer formula $[M^{(II)}_{1-x}M^{(III)}_{x}(OH)_2]^{x+}$. This excess positive charge is compensated by anions intercalated between the brucite layers, with intercalated molecular water providing hydrogen bonding between the layers. In addition to numerous synthetic LDH compounds, some of them with extensive industrial applications, > 40 LDH-type mineral species are known, with hydrotalcite, $Mg_6Al_2(OH)_{16}[CO_3]\bullet 4H_2O$, as the name-giving mineral of this super group of minerals (Mills et al. 2012). The structural arrangements confers LDH the interesting property of accommodating and immobilizing a wide range of cations (e.g. Mg^{2+}, Fe^{2+}, Ni^{2+}, Co^{2+}, Zn^{2+}, Al^{3+}, Fe^{3+}, Eu^{3+}, Cr^{3+}, Zr^{4+}) as well as inorganic and organic anions (e.g. I^-, Br^-, Cl^-, CO_3^{2-}, SO_4^{2-}, carboxylates, sulfonates, or dicarboxylates) in the brucite layer and the interlayer, respectively (Carteret et al., 2011; Curtius et al., 2008; Johnson and Glasser, 2003; Aramendia et al., 2002; Carlino et al., 1997; Cavani et al., 1991; Chibwe et al., 1989; Carrado et al., 1988; Brindley et al., 1980; Boclair et al., 1999; Miyata et al., 1973).

In deep geological repository systems for radioactive wastes, LDH are expected to be present in various forms and may provide a retention potential especially also for anionic species of long-lived safety relevant radionuclides such as ^{129}I, ^{99}Tc, ^{79}Se, ^{36}Cl and ^{14}C (Aimoz 2013; Aimoz 2012a,b; Curtius et al., 2008; Curtius and Kattilparampil, 2005; Allada et al. 2005a; Johnson and Glasser, 2003). For example, Fe^{II}/Fe^{III}-LDH, commonly termed "green rust", can form as (intermediate) anaerobic corrosion products of steel waste canisters (Refait and Genin, 1993; Wersin et al., 2003; Wersin et al., 2014). Mg-Al-Cl-LDH were found as secondary phases forming in corrosion experiments on metallic dispersion-type research reactor fuel plates in Mg-rich brines and clay waters (Curtius et al. 2009, Klinkenberg et al. 2014, Neumann et al. 2016). In alteration experiments performed by Abdelouas et al. (1994), hydrotalcite-like compounds were observed as crystalline secondary phases on the surface of nuclear waste glasses. Ca-Al-Cl-LDH like Friedel´s salt ($Ca_2Al(OH)_6(Cl,OH)•2H_2O$) are known to form during the corrosion of cemented wastes in salt brines (Fernández et al., 2010). Moreover, Ca-Al-LDH termed AFm as well as small amounts of hydrotalcite are generally present as hydration products in cementitious materials used, for example, as construction and support materials or in the engineered barrier system in deep geological repositories (Taylor 1997; Glasser 1997).

The introduction of LDH phases in geochemical models addressing the retention of radionuclides or other contaminants is generally hampered by the lack of knowledge on their thermodynamic properties. Moreover, LDH span a wide compositional range and have to be considered as complex multicomponent solid solutions potentially incorporating various cations and anions. So far, few studies have been dedicated to the evaluation or prediction of the thermodynamic properties of LDH. For example, Boclair and Braterman (1999) titrated solutions containing di- and trivalent metal chlorides (M(II) = Mg^{2+}, Zn^{2+}, Co^{2+}, Ni^{2+}, Mn^{2+}; M(III) = Al^{3+}, Fe^{3+}) with

NaOH and determined nominal solubility constants for the various precipitating LDH from an analyses of the titration curves. Based on the results of high temperature oxide melt solution calorimetry, Allada et al. (2005a,b) summarized the thermodynamic properties of hydrotalcite $Mg_{0.74}Al_{0.026}(OH)_2(CO_3)_{0.13}\cdot 0.39H_2O$ and determined the enthalpies of formation of Mg-Al-LDH intercalated with Cl^-, I^-, NO_3^-, ReO_4^- or CO_3^{2-}. Subsequent studies using similar methods addressed the standard enthalpies of formation for M(II)-Al-LDH (M(II) = Mg^{2+}, Co^{2+}, Ni^{2+} or Zn^{2+}) with CO_3^{2-} as interlayer anion (Allada et al. 2006). Johnson et al. (2003) synthesized hydrotalcite-like phases with similar composition and estimated their solubility products in dissolution experiments. Recently, Rozov et al. (2010, 2011, and 2013) and Curtius et al. (2013) investigated the effects of the isostructural incorporation of different cations on the stability of layered double hydroxides. In these studies the standard molar Gibbs free energies of formation of various Mg^{2+}, Fe^{2+}, Co^{2+}, Ni^{2+} Al^{3+}, and Fe^{3+} bearing LDH were estimated based on Gibbs Energy Minimization.

The present study focuses on the synthesis and characterization of Zr(IV)-bearing Mg-Al-LDH containing Cl^- as interlayer anion, and the derivation of their thermodynamic properties. Zirconium alloys ("zircaloys") are used extensively in the nuclear industry, for example as cladding material for fuel rods in water cooled nuclear reactors, due to their low neutron cross-sections, appropriate thermal conductivity, as well as high corrosion resistance and mechanical stability. During reactor operation, the long-lived radionuclide ^{93}Zr (half-life 1.53 million years, ENDF/B-VII.1, Chadwick et al., 2011) is formed from stable ^{92}Zr present in the reactor components by neutron activation (n,γ-reaction). Moreover, ^{93}Zr is generated as a significant fission product due to the thermal fission of ^{235}U in the nuclear fuels (cumulative fission yield 6.35%, ENDF/B-VII.1, Chadwick et al., 2011). Thus, ^{93}Zr is present in spent nuclear fuels and in

high-level radioactive waste resulting from their processing (i.e. nuclear waste glasses and compacted hulls and end pieces), as well as in other secondary wastes associated with the reprocessing of spent nuclear fuels. In a repository environment, the formation of Zr-bearing LDH could provide a means of retaining/immobilizing ^{93}Zr. However, in order to be able to account for the potential Zr-retention by solid solution formation with LDH in safety assessments, reliable thermodynamic data for these phases are required.

In earlier studies, Zr-LDHs were synthesized with either Cl^- or CO_3^{2-} as interlayer anions. In general, the incorporation of Zr(IV) or other tetravalent metals in LDH as partial substitution of Mg(II) or Al(III) was thought to be difficult due to its higher valence (Velu et al. 1998; Shen et al. 2011). Velu et al. (1998) synthesized carbonate-bearing Zr-Mg-Al- and Zr-Zn-Al-LDH by co-precipitation methods, whereas Curtius et al. (2009) incorporated Zr(IV) in Mg-Al-Cl-LDHs. However, the structural incorporation of Zr(IV) into the brucite layers was strongly debated. By combining X-ray absorption spectroscopy (XAS) and Mössbauer spectroscopy, Intissar et al. (2003) demonstrated that tetravalent cations such as Zr(IV) may segregate from the structure of Mg-Al-LDH and Co-Al-LDH and form amorphous M(IV)-oxide-like particles. More recently, Shen et al. (2011) synthesized Zr-Mg-Al-CO_3-LDH and demonstrated that up to 10 mol% Zr(IV) can be incorporated into the brucite layers of LDH. Rozov et al. (2015) synthesized Zr-LDH by co-precipitation methods and found that the crystallinity of the LDH structures is likely to decrease with the Zr-content. The authors also estimated for the first time the standard Gibbs energy of formation of Zr-Mg-Al-Cl-LDH based on a Gibbs free energy minimization approach. However, a complete thermodynamic description of Zr-LDH validated by experimental measurements is lacking so far.

133 Moreover, all thermodynamic data on Zr-LDH available up to now have been estimated for
134 standard conditions (T=293.15 K, P =1 bar). However, in the case of deep geological disposal of
135 highly radioactive and heat-generating nuclear wastes, elevated temperatures are expected in the
136 repository near-field over some hundreds of years (thermal phase), due to the high decay heat
137 produced by short-lived radionuclides in the waste. If an early failure of waste canisters occurs,
138 radionuclides may come into contact with aqueous systems at higher temperature conditions.
139 Therefore in this study we investigate the incorporation of Zr(IV) in Mg-Al-LDH at different
140 temperatures, to (i) explore the limits of substitutional Zr(IV) uptake as function of temperature,
141 and (ii) to determine relevant thermodynamic properties of the Zr-LDH, with the aim of
142 improving the scientific basis for assessing nuclear waste disposal scenarios at elevated
143 temperatures. For this purpose Zr-Mg-Al-LDH with different compositions were synthesized by
144 a coprecipitation method in the temperature range from 293 to 343K, characterized, and their
145 thermodynamic properties (e.g. Gibbs energy of formation, entropy and enthalpy of formation,
146 etc.) determined by complementary theoretical and experimental approaches. This approach
147 aimed at both extending the thermodynamic database for the long-lived fission product ^{93}Zr at
148 elevated temperatures, as well as testing estimation methods for thermodynamic data and model
149 parameters and their experimental validation.

150 **2 Material and Methods**

151 **2.1 Synthesis and characterization**

152 **2.1.1 Synthesis**

153 Samples of Mg-Al-Zr-Cl-LDH solids with two different Zr/(Zr+Al) ratios of 0.1 (series 1) and
154 0.4 (series 2) were synthesised at different temperatures (T = 298, 313, 323 and 343 K) at pH of

10.00 ± 0.05 by a co-precipitation method. The synthesis procedure, previously described in Rozov et al. (2015), comprises the slow addition (addition rate 0.2 to 0.3 mL min^{-1}) of 40 mL degassed metal chloride solution with a metal ratio Mg/(Al+Zr) ~ 3:1 into a reactor vessel filled with 250 mL degassed boiled MilliQ water under stirring and under argon gas flow. The total metal concentration in the chloride solution was 0.8 M. Simultaneously the pH was maintained at 10.00 by the addition of a 2 M NaOH solution using an automated titrator 736 GP TITRINO (Metrohm). After the addition step, the stirring of the suspension was continued for 24 hours (aging time) while keeping the pH controlled at 10.00 ± 0.05 and maintaining a constant synthesis temperature. The precipitates and the supernatant liquid were separated by filtration. The solids were washed three times with boiled degassed MilliQ water and finally dried in a desiccator at 60°C for 24 hours to remove physically adsorbed water. The synthesis procedure was carried out under argon flow to avoid carbonate contamination.

2.1.2 Material characterization

The contents of Mg, Al and Zr in the aqueous solutions after synthesis and in the solids were determined by ICP-OES using a TJA-IRIS™ instrument, the Cl content was determined using ionic chromatography. Prior to dilution for chemical analysis, the supernatant after synthesis was filtered using Millipore Milliex-HV Hydrophilic PVDF 0.45 µm filters to remove colloids. The solids were dissolved in 2 M HNO_3 (20 mg in 2 mL acid) prior to analysis. The amounts of OH^- in the solids were calculated assuming charge neutrality.

Thermogravimetric and differential scanning calorimetry (TGA-DSC) analyses of the solids were carried out with a Netzsch STA 449 C Jupiter™ instrument to determine the interlayer water content of the LDH. The analyses were performed from 298 K to 873 K at a heating rate of 10 K min^{-1} under synthetic air flow (flow rate 30 mL min^{-1}).

Infrared spectra of the precipitates were obtained with a FT-IR Bruker Equinox 55 instrument using the KBr pellet method in order to identify the interlayer composition. Spectra were recorded in the wavenumber interval from 400 cm^{-1} to 4000 cm^{-1}.

Powder X-ray diffraction (XRD) on a Bruker D4 diffractometer (Bragg-Brentano geometry) was carried out with Cu K_α radiation (λ Cu K_α = 1.5418 Å) at ambient temperature within a 2θ-range from 5 to 80° with a step size of 0.02° 2θ and dwell time of 1s, to confirm the nature and crystallinity of the synthesized LDH. The unit-cell parameters ($a_0 = b_0$ and c_0) of the Zr-LDH solids were estimated by applying Bragg's law and using relations between specific indexed interplanar distances d_{hkl} and lattice unit-cell parameters for hexagonal symmetry. The lattice parameters a_0 and c_0 were calculated as follows: $a_0 = 2\times d_{110}$ and $c_0 = 3\times d_{003}$.

Scanning electron microscopy (SEM) examinations of the samples were carried out in low vacuum mode at 60 Pa, using a FEI Quanta 200F electron microscope equipped with EDX (Apollo X silicon drift Detector, EDAX), to investigate the morphology of the synthesized solids and to obtain information on their chemical homogeneity. EDX analyses were carried out at an accelerating voltage of 20 kV and a working distance of 10 mm.

2.2 Determination of solubility of LDH

The solubility as function of temperature was evaluated by determining the ion activity product at the different synthesis temperatures after sufficient equilibrium time.. The synthesized LDH of the general composition $Mg_xAl_yZr_z(OH)_2Cl_{(2x+3y+4z-2)}$ is in equilibrium with the solution as follows:

$$LDH = xMg^{2+} + yAl(OH)_4^- + zZr(OH)_4 + (2-4y-4z)OH^- + (2x+3y+4z-2)Cl^- \quad (1)$$

The equilibrium constant (stoichiometric saturation constant) K(LDH) of the LDH at the experimental condition of pH=10.0 ± 0.05 can therefore be calculated using eq. (2):

$$K(LDH) = \left(\gamma_{Mg^{2+}} c_{Mg^{2+}}\right)^{x} \cdot \left(\gamma_{Al(OH)4^{-}} c_{Al(OH)4^{-}}\right)^{y} \cdot \left(\gamma_{Zr(OH)4} c_{Zr(OH)4}\right)^{z} \cdot \left(\gamma_{OH^{-}} c_{OH^{-}}\right)^{2-4y-4z} \cdot \left(\gamma_{Cl^{-}} c_{Cl^{-}}\right)^{2x+3y+4z-2} \quad (2)$$

where γ_i and c_i are the activity coefficient and molal concentration of the main aqueous species in solution at pH =10. The activity coefficients for all dissolved species were calculated according to the extended Debye-Hückel model (Helgeson et al. 1981). The application of this activity model, of which a detailed description is provided in Wagner et al. (2012), is justified by the relatively low ionic strength of the solution at equilibrium (ionic strength ~ 0.2).

2.3 Theoretical approach to estimate the standard Gibbs energies of synthesized Zr-containing LDHs

The thermodynamic modelling was performed assuming thermodynamic equilibrium between the precipitates and the aqueous solutions after synthesis.

Gibbs energy minimization (GEM) approaches implemented in the GEMS3K solver (http://gems.web.psi.ch/GEMS3K) and described in Kulik et al. (2013) were used to estimate molar Gibbs free energies of formation of the Zr-LDH at various temperatures (T= 298, 313, 323 and 343 K). Thermodynamic data were taken from the PSI-Nagra chemical thermodynamic database 12/07 (Thoenen et al., 2014) that includes the data for aqueous Zr-species and Zr-bearing solids from the OECD-NEA review (Brown et al. 2005). The measured chemical compositions of the aqueous phases after synthesis were used as input in GEMS3K to calculate speciation and activities of dissolved metals and anions, in order to determine the chemical

potentials of relevant components. At thermodynamic equilibrium, the Gibbs free energy of the system is minimal and the chemical potentials of the components in each phase are the same. Hence, the free Gibbs energies of formation ΔG_f° can be computed using the following eq.:

$$\Delta G_f^\circ(Zr-LDH) = a\mu(Mg^{2+}) + b\mu(Al^{3+}) + c\mu(Zr^{4+}) + d\mu(OH^-) + e\mu(Cl^-) \quad (3)$$

where a-e are stoichiometric coefficients and μ(i) are the calculated chemical potentials.

2.4 Experimental approach to evaluate the thermodynamic properties of Zr-containing LDHs

2.4.1 Dissolution calorimetry

The enthalpy of dissolution of the Zr-LDH at 298 K was measured in a Calvet-type calorimeter (Setaram-C80) using an acidic solvent. The calorimeter apparatus consists of two cells, a reference cell and a sample cell, placed in the calorimetric containment. An optimum solid to solvent volume ratio (10 mg in 5 mL solution) was chosen such that the dissolution is efficient, fast and produces a significant thermal signal. Both cells were thermally equilibrated for 3 hours before each measurement. During this time, the heat flow variation did not exceed 0.01 mW at 298 K. Both sample holders (from the reference and measuring cell) were then simultaneously ejected into the lower cell compartments marking the start of the dissolution process. As the reaction proceeds, the heat flow is recorded as function of time for about 8 hours, after which the heat flow reaches the background noise of ~0.01 mW. The measured heat effect (enthalpy of dissolution, ΔH_{diss}) was obtained by integrating the heat flow curve using the CALISTO software provided by Setaram. Prior to the measurements, the calorimeter was calibrated using an analogous reaction i.e. the heat released during the dissolution of KCl in water at 298 K.

For a better evaluation of the enthalpy of formation, the dissolution in two different solvents i.e. hydrochloric acid (HCl) and nitic acid (HNO_3) was tested. The measured enthalpy of formation was then computed following method 1 and method 2 described below.

Method 1: Based on the dissolution reaction in 1 M HCl given in eq. (4), the standard enthalpy of formation, ΔH_f^0(LDH), is obtained using eq. (5) whereby the enthalpy of dissolution ΔH_{diss}° (LDH/HCl) equals the measured heat of the dissolution reaction.

$$Mg_xAl_yZr_z(OH)_2Cl_{2x+3y+4z-2}.mH_2O_{(s)} + 2HCl \rightarrow xMg^{2+}{}_{(aq)} + yAl^{3+}{}_{(aq)} + zZr^{4+}{}_{(aq)} + (2x+3y+4z)Cl^{-}{}_{(aq)} + (2+m)H_2O_{(l)} \quad (4)$$

$$\Delta H_f^{\circ}(LDH) = \sum a_i H_f^{\circ}(aqeous\ species) - \Delta H_{diss}^{\circ}(LDH/HCl) \quad (5)$$

where H_f° is the standard enthalpy of formation of the aqueous species. Eq. 4 assumes that no complexation occurs and the cations exist as free ions at low pH.

Method 2: The standard enthalpies of formation of the synthesized LDHs were also computed from the heat effect associated with the dissolution in 1 M HNO_3 at 298 K. Because the complexes (and associated energies of formation) between the nitrates and the cations constituting the synthesized LDH were not known, the solution enthalpies of each cation hydroxide/chloride had to be measured individually. Table 1 shows the thermocycle used to calculate the ΔH_f° of the synthesized LDH from the single cation hydroxide and chlorides. The enthalpy of formation of ions as well as of metal chlorides and hydroxides used in the calculation of the enthalpy of formation are given in Table 2. Although the dissolution in HNO_3 introduces various errors (due to the multiple steps) in the final enthalpy of formation results, it can still be used to validate the results computed from the enthalpy of LDH dissolution in HCl.

Table 1: Thermocycle for calculating enthalpy of formation.

data Dissolution in 1M HNO_3(complexes with HNO_3 are not shown here)		Eq.
ΔH_{diss}° (LDH/HNO_3)	$Mg_{(x)}Al_yZr_z(OH)_2Cl_{2x+3y+4z-2}.mH_2O \rightarrow xMg^{2+} + yAl^{3+} + zZr^{4+} + (2x+3y+4z-2)Cl^- + 2OH^-_{(aq)} + mH_2O$	(6)
$\Delta H1$	$Mg(OH)_{2(s)} \rightarrow Mg^{2+}_{(aq)} + 2OH^-_{(aq)}$	(7)
$\Delta H2$	$MgCl_2.6H_2O_{(s)} \rightarrow Mg^{2+}_{(aq)} + 2Cl^-_{(aq)} + 6H_2O_{(l)}$	(8)
$\Delta H3$	$AlCl_3.6H_2O_{(s)} \rightarrow Al^{3+}_{(aq)} + 3Cl^-_{(aq)} + 6H_2O_{(l)}$	(9)
$\Delta H4$	$ZrOCl_2.8H_2O_{(s)} + H^+ \rightarrow Zr^{4+}_{(aq)} + 2Cl^-_{(aq)} + OH^- + 8H_2O$	(10)
Precipitation of LDH from salts		(11)
$\Delta_r H$	$Mg_{(x)}Al_yZr_z(OH)_2Cl_{2x+3y+4z-2}.mH_2O \rightarrow Mg(OH)_{2(s)} - (1-x)MgCl_2.6H_2O_{(s)} + yAlCl_3.6H_2O_{(s)} + zZrOCl_2.8H_2O_{(s)} + 2zCl^-_{(aq)} - (z/2)O_2(aq) - (m-6+6x+6y+8z)H_2O$	(12)
$\Delta H_f^{\circ}(LDH) = \sum a_i H_f^{\circ}(salts\ and\ aqeous\ components) - \Delta_r H$		(13)
where $\Delta_r H = \Delta H1 - (1-x)\Delta H2 + y\Delta H3 + z\Delta H4 - \Delta H_{diss}^{\circ}$ (LDH/HNO_3)		(14)

Table 2: Enthalpies of formation of ions and solids used in the calculations of the standard enthalpy of formation of Zr-LDH.

Species	**ΔH_f^0 (kJmol^{-1})**	**Source**
$Al^{3+}_{(aq)}$	-530.630	Shock et al., 1997
$Mg^{2+}_{(aq)}$	-465.929	Shock et al., 1997
$Zr^{4+}_{(aq)}$	-628.901	Shock et al., 1997
$Cl^-_{(aq)}$	-167.111	Shock et al., 1997
$OH^-_{(aq)}$	-230.009	Shock et al., 1997
H_2O	-285.881	Johnson et al., 1992
$O_{2(aq)}$	-12.237	Shock et al., 1989
$Mg(Cl_2).6H_2O$	-2498.9±0.8	Shomate and Huffmann, 1943
$AlCl_3.6H_2O$	-2691.6±1.3	Coughlin, 1958
$ZrOCl_2.8H_2O$	-3468.536	Chevaunet, 1913
$Mg(OH)_{2(s)}$	-923.272	Helgeson et al., 1978

2.4.2 Low-temperature adiabatic calorimetry

The heat capacities of the LDH were measured with a Quantum Design Physical Properties Measurement System (PPMS). A powder sample (~10 mg) of LDH was compressed into a small Cu crucible. The accuracy of the mass determination was about ±0.02 mg. The heat capacity of the Cu crucible was determined separately and subtracted from the total measured heat capacity. At each temperature three responses to a heat pulse were measured and analyzed with the software MultiVu (Quantum Design Inc., San Diego, CA, USA).

Data were collected upon cooling the sample from 300 K to 2 K at 145 temperature points. Then the sample was heated to 250 K and the heat capacity was measured upon heating the sample from 250 K to 350 K at 15 temperature points. The temperature difference between subsequent steps was increased logarithmically from low to high temperatures.

The calibration of the heat capacity measurements was performed by measurements of Al_2O_3 (SRM-720) and Cu (99.999%, Alfa Aesar) reference materials. A comparison of our data for SRM-720 with those published by Ditmars et al. (1982) gives a deviation of 2% in the range between 395 and 50 K and 6% below 5 K. The heat capacity data of the Cu sample were compared with those of Lashley et al. (2003); the deviation is less than 1% in the temperature range between 300 and 40 K and ~2% below 40 K.

3 Results and Discussion

3.1 Synthesis and characterization

3.1.1 Structural properties of synthesized solids

Powder XRD was used to check whether all synthesised precipitates were pure Zr-LDH phases and that all Zr was structurally incorporated into the LDH. Fig. 1 depicts the diffractograms of all synthesised Zr-LDH, displaying only diffraction patterns typical for LDH phases. This indicates that the amounts of potential crystalline impurities in the precipitates (e.g. brucite or Al-oxides/hydroxides) are below the limit of detection of XRD. Moreover, no broad features, characteristic of the presence of amorphous phases, were observed. For series 2 LDH Zr/(Al+Zr) = 0.4, although the diffractograms shown in Fig. 1 have similar characteristics as series 1 LDH, a decrease in the peak intensity at $2\theta = 60°$ and the loss of a shoulder at the right part of the peak

296 were observed which may be taken as an indication of a decrease in crystallinity. The calculated
297 lattice parameters for all synthesised Zr-LDH are provided in Table 3.

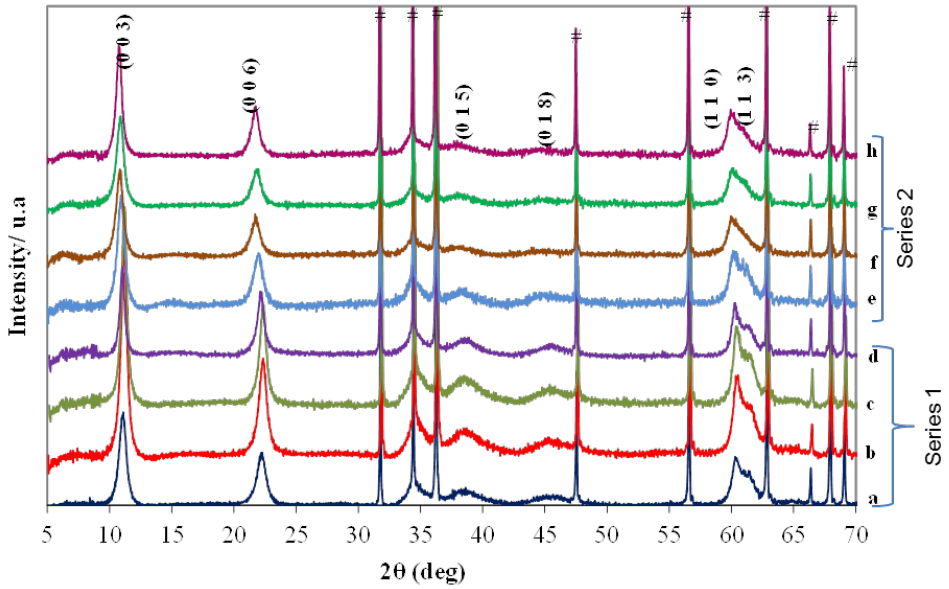

298

299 **Fig 1:** XRD patterns of synthesized LDH (a) LDH-S1-293K, (b) LDH-S1-313K,(c) LDH-S1-
300 323K, (d) LDH-S1-343 K, (e) LDH-S2-293K, (f) LDH-S2-313K, (g) LDH-S2-323K, (h) LDH-
301 S2-343K where S1 refers to series 1 (Zr/(Al+Zr) = 0.1) and S2 to series 2 (Zr(Al+Zr) = 0.4) (#
302 denotes peaks from ZnO internal standard).

303 The lattice parameter a_0 corresponds to the cation-cation distance in the brucite-like layers. c_0
304 represents the layer spacing that depends on the charge density of the brucite layer and the
305 characteristics of the interlayer anion. As expected, the lattice parameter a_0 increases with
306 increasing incorporation of Zr^{4+} in the brucite layer,indicating that the cation-cation distance
307 expands due to the substitution of Zr^{4+} ($r(Zr^{4+})$ = 0.720 Å) for the smaller Al^{3+} ion ($r(Al^{3+})$ =
308 0.535 Å). However, the lattice parameter a_0 of the Zr-LDH is rather similar to the values reported
309 for Zr-free Cl-intercalated Mg-Al-LDHs in the literature (Curtius et al. 2005; Rozov et al., 2013).

Table 3: Calculated lattice parameters for Zr-LDH compared to literature data for Mg-Al-Cl-LDH. Estimated errors are 1 K for the synthesis temperature and 0.005 and 0.005 Å for the lattice parameters.

Material	Synthesis conditions		lattice parameters	
	Zr/(Zr+Al) [-]	Temperature [K]	a_0 [Å]	c_0 [Å]
Mg-Al-Zr-Cl-LDH	0.1	298	3.063	23.997
	0.1	313	3.061	24.034
	0.1	323	3.066	24.121
	0.1	343	3.067	24.176
	0.4	298	3.069	24.248
	0.4	313	3.075	24.494
	0.4	323	3.072	24.388
	0.4	343	3.078	24.652
Cl-Hydrotalcite[a]	-	298	3.082	24.065
Cl-Hydrotalcite[a]	-	343	3.066	23.959
Mg-Al-Cl-LDH[b]	-	363	3.06	24.165

a: Rozov et al. 2013, b: Curtius et al. 2005

The values of the lattice parameter c_0 increase with increasing Zr content, showing that the layer spacing increases. The incorporation of Zr^{4+} ions into the brucite layers increases their net positive charge and should therefore increase the attraction to the interlayer anions. This would consequently induce a decrease in the interlayer distance. However, in our study, the opposite result is observed. This can be attributed to an increase in the thickness of the brucite layer upon the incorporation of Zr^{4+}, and/or the accommodation of a larger amount of hydrated anions in the interlayer (Velu et al. 1998, Shen et al. 2011). A similar increase in the lattice parameter c_0 with increasing Zr-content in Mg-Al-LDH was also observed by Rozov et al. (2015).

3.1.2 Microstructure and impurities of synthesized solids

SEM observations showed that both series of LDH exhibit aggregates of platy crystals < 1 µm typical for LDH (Fig. 2). In order to investigate the homogeneity of the samples, back scattered electron (BSE) images were taken and EDX spot measurements were conducted (Fig. 3a and 3b). The BSE images of the series 1 LDH (Zr/(Zr+Al) = 0.1) indicate a homogenous distribution of

Zr in the solid. This was confirmed by EDX spot analysis, whereby the peak intensities and thus Zr atomic concentrations are the same in different regions (Zr/(Zr+Al+Mg) = 0.02). In contrast, BSE images of series 2 LDH (Zr/(Zr+Al)=0.4) showed a heterogeneous distribution of Zr (Fig. 4a and b), with Zr-rich areas indicated by brighter contrast. Corresponding EDX analyses showed varying chemical compositions. This confirms the formation of a segregated Zr-rich phase, possibly an amorphous hydrous Zr-oxide (Intissar et al., 2003), since this phase was not distinguishable from LDH by XRD. The BSE SEM observation from series 2 suggest an increase in the amount of the amorphous Zr-phase with temperature (increase of bright phase), which can be explained by the decrease in solubility of hydrous Zr-oxides with temperature. The quantification of the amorphous phase using EDX was however not possible as the data collected represent an average of the composition of the interaction volume of the electron beam with the sample, which is large compared to the particle size. However, regions within an area of homogeneous contrast showed 5±1 atomic % of Zr, which could be regarded as an estimate for the maximum Zr-uptake in the LDH structure.

Infrared spectroscopy was performed to characterize the nature of interlayer anions and to investigate their interaction with the octahedral brucite-like layers. Fig. 5 exemplarily shows the FT-IR spectra of the Zr-LDH samples synthesised at 343 K. All samples contained a broad strong absorption band around 3460 to 3470 cm^{-1} corresponding to the ν_{OH} stretching vibration of the brucite-like layers (Shen et al., 2011) . The absorption band around 800 cm^{-1} is attributed to the Mg-Al-O vibration in the brucite like layer, while bands around 600 cm^{-1} are assigned to M-O stretching and bending vibrations (Shen et al., 2011). A weak band around 1630 cm^{-1} is ascribed to the $\delta_{H\text{-}OH}$ vibration of the interlayer water. A weak band at 1370 cm^{-1} is attributed to the ν_3 asymmetric stretching vibration of CO_3^{2-} anions. The presence of carbonate ions in the

precipitates can be explained by the uptake of small amounts of atmospheric CO_2 during sample preparation and IR-measurements, due to the very strong affinity of LDHs for this compound. However, we assume that all the LDH samples are initially carbonate free since the co-precipitation and storage were carried out under argon atmosphere.

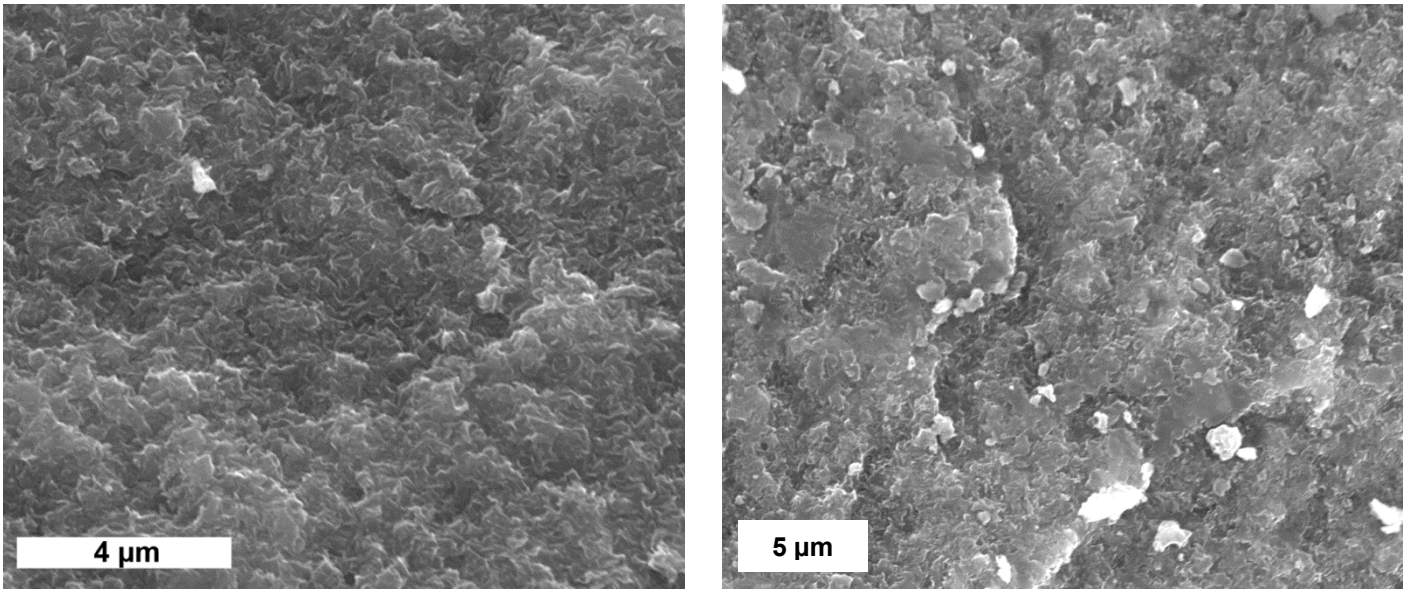

Fig. 2: Secondary electron (SE) image of LDH-S1-243K and LDH-S2-243K.

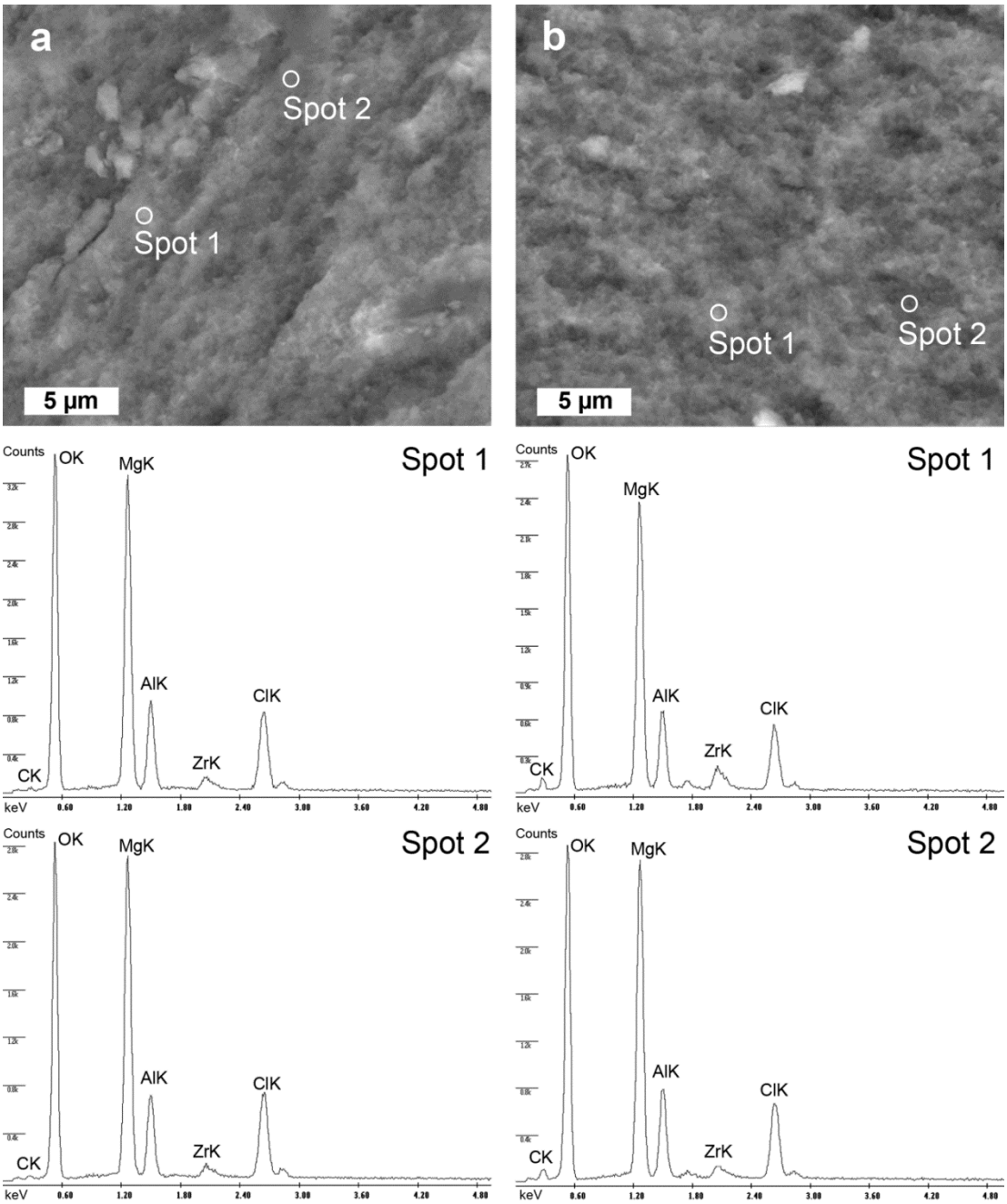

Fig. 3: BSE-SEM images coupled with EDX analysis of Zr-LDH (nominal Zr/(Zr+Al) = 0.1) synthesised at 323 K (a) and at 343 K (b).

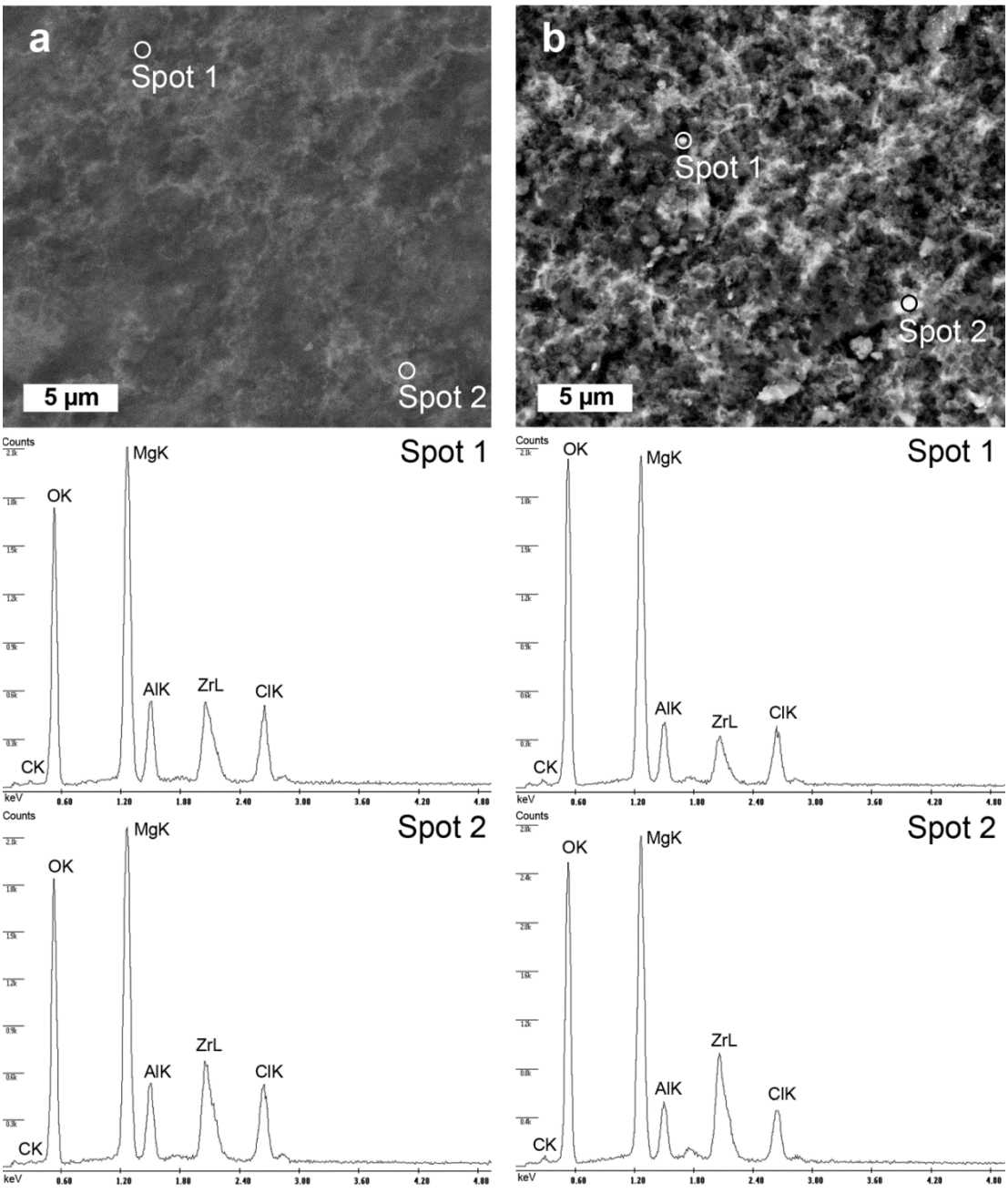

Fig. 4: BSE-SEM images coupled with EDX analysis of Zr-LDH (nominal Zr/(Zr+Al) = 0.4) synthesised at 298 K (a) and 343 K (b).

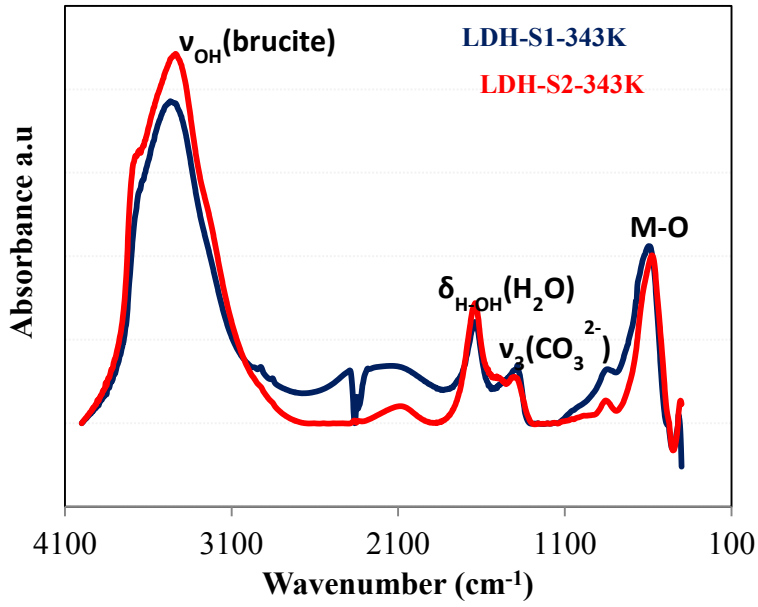

361

362 **Fig. 5:** Representative FT-IR spectra of synthesized Zr-LDH with nominal Zr/(Zr+Al) = 0.1

363 (blue curve) and Zr/(Zr+Al) = 0.4 (red curve).

364 **3.1.3 Stoichiometry of the solids**

365 For series 1 (nominal Zr/(Zr+Al)= 0.1), the synthesis of the LDH at a given temperature was

366 repeated at least three times; the average elemental composition of the solids ($Mg_{(x)}Al_yZr_z(OH)_2$

367 $Cl_{2x+3y+4z-2}.mH_2O$) for each synthesis temperature were calculated and is given in Table 4. Each

368 sample was found to bear an $M^{2+}/(M^{3+}+M^{4+})$ ratio close to the starting one in solution of ratio 3.0

369 ± 0.1 as was previously reported by Aimoz et al. (2013). The composition and stoichiometry of

370 the solid was found to be invariant with temperature.

371 Series 2 LDH consisted of a mixture consisting of LDH presumably containing an amorphous

372 phase of hydrous Zr-oxide. Therefore the chemical composition of these solids and the solution

373 at equilibrium are not reported here. Based on EDX spot analysis, we estimate that a maximum

374 Zr uptake of 0.05 mol per unit mol of LDH was achieved in our syntheses. This is lower than the

maximum Zr-uptake (0.125 mol per unit mol of LDH) obtained by Rozov et al. (2015) for Cl-bearing LDH prepared by a similar syntheses route. Beyond this value, these authors observed a decrease in the crystallinity of the LDH. However, it should be noted that the observations of Rozov et al. (2015) were purely based on XRD analysis, whereby the presence of amorphous phases were not discussed, although a high background is visible in all their XRD patterns. Our estimated maximum Zr-uptake in Cl-bearing LDH is lower than the 0.10 mol of Zr that can be structurally incorporated in a CO_3^{2-} bearing LDH (Shen et al., 2011). Therefore, it is most likely that the interlayer anions can influence the Zr uptake. Carbonate ions have a higher charge density than chloride ions, what could possibly contribute to an increase in stability of carbonate-bearing Zr-LDH.

Table 4: Stoichiometries of Zr-LDH ($Mg_xAl_yZr_z(OH)_2\ Cl_{2x+3y+4z-2}.mH_2O$) phases from series 1 (Zr/(Zr+Al) = 0.1) determined by chemical analysis. The error is the calculated standard deviation from the samples for each temperature.

Synthesis Temperature [K] ±1	Mg^{2+} ±0.01	Al^{3+} ±0.01	Zr^{4+} ±0.005	OH^-	Cl^- ±0.01	H_2O ±0.03
298	0.71	0.22	0.025	2	0.21	0.67
313	0.72	0.23	0.024	2	0.20	0.64
323	0.73	0.21	0.025	2	0.21	0.63
343	0.72	0.21	0.024	2	0.20	0.70

Thermogravimetric analyses coupled with differential scanning calorimetric measurements revealed a typical stepwise thermal decomposition of hydrotalcite-like solids (Rives 2002, Vágvölgyi et al. 2008) and were applied to determine the amount of structurally bound water. Fig. 6 shows representative TGA-DSC curves of Zr-LDH samples with both low and high content. The first endothermic peak at around 408 K and 433 K corresponds to the loss of the interlayer water molecules. The average stoichiometric water content in the synthesised solids

was determined to be 0.65±0.04 for series 1 LDH. The second endothermic peak at around 643 K and 673 K corresponds to the loss of hydroxyl groups. This weight loss corresponds to a stoichiometric content of hydroxyl ions of 2.1±0.1 in the LDH. Since additional transformations (e.g. including chloride decomposition (Galwey and Laverty, 1989) take place in this temperature range, the OH content of the Zr-LDH may be slightly overestimated. Thus the total amount of OH- in chloride-LDH is usually not determined by TG measurements. The higher weight loss of Zr-LDHs with the higher Zr content during the first decomposition step indicates a higher amount of interlayer water in these precipitates or a potential contribution of the dehydration of the hydrous Zr-oxide. The shift of the first and second weight loss to lower temperatures for these LDH suggests that the thermal stability decreases with an increase in Zr in the brucite layer.

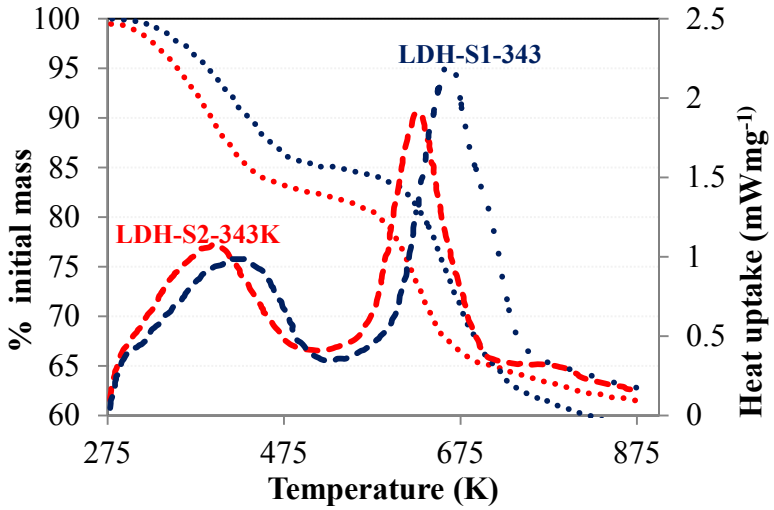

Fig 6: TGA-DSC curves of Zr-LDH with xZr = 0.1 (blue) and xZr = 0.4 (red) synthesised at 243 K. The right axis corresponds to the % of initial mass (dotted line) while the right axis refers to the heat uptake during the decomposition (dashed lines).

In summary it can be concluded that Zr can be incorporated in the brucite layer and forms well crystalline structure up to a certain limit of Zr, beyond which an amorphous phase of hydrous zirconium oxide will precipitate. It is known that solution conditions, namely the relative cation activities and pH are important in controlling the composition of the LDH phases (Allada et al., 2005b). However, it seems that temperature has no great impact on the stoichiometry of the precipitating LDH phase. Our synthesized LDH (series 1) have generally the stoichiometry $Mg_{0.72}Al_{0.22}Zr_{0.025}(OH)_2Cl_{0.20}*mH_2O$ with m = 0.65 ± 0.04. The solubility of the LDH as a function of the temperature and the thermodynamic properties of this compound are evaluated in the following sections.

The LDH is further considered as a phase of fixed composition rather than a member of a solid solution series. Thus we assume that a hypothetical field of stability of Zr-LDH within the ternary composition space of brucite ($Mg(OH)_2$), baddeleyite (ZrO_2) and gibbsite ($Al(OH)_3$) is represented by a single point. This assumption imposes limitations on possible geochemical applications of our results, because at equilibrium under open conditions the LDH phase should be able to change it composition within its field of stability. Our assumption forbids such a change. For a more realistic description of Zr-LDH solid solution series, synthesis with a variation in Al/Zr ratio has to be considered. Our attempt to increase the Zr/Al ratio in this work resulted in the formation of a mixture of LDH and amorphous phase of hydrous Zr-oxide as the maximum Zr uptake in the brucite sheet was exceeded.

3.2 Solubility of LDH as function of temperature

The stoichiometric saturation constant of the Zr-LDH ($Mg_{0.72}Al_{0.22}Zr_{0.025}(OH)_2Cl_{0.20}$) was determined from the composition of the syntheses solutions. The ionic concentrations of the solutions after reaction as well as the derived equilibrium constants (calculated using eq. 2) are

presented in Table 5. The aqueous concentration of cations in solution decrease with the increasing temperature. Thus the solubility of the LDH decreases also with temperature (lnK(298 K) = -17.5 and lnK(343K) = -19.7 calculated at pH = 10 using eq. 2); which is common characteristic of metal hydroxides (Lydersen, 1990).

In Fig. 7 (the Van't Hoff plot) the stoichiometric saturation constant is plotted as function of the inverse temperature 1/T(K). The stoichiometric saturation constant can be expressed as function of the enthalpy of reaction, $\Delta_r H^\circ$, and the entropy of reaction $\Delta_r S^\circ$ as follows:

$$lnK(T) = \left(\frac{-\Delta_r H^\circ}{R}\right)\frac{1}{T} + \frac{\Delta_r S^\circ}{R} \qquad (15)$$

where $\Delta_r H^\circ$ and $\Delta_r S^\circ$ were calculated from the slope of the line and intercept respectively. It should be noted that the experimental point at 213 K was discarded for a better linear regression. The calculated negative $\Delta_r H^\circ$ of -412±14 kJ mol^{-1} indicates an exothermic reaction; $\Delta_r S^\circ$ was determined to be -4.00±0.06 J mol^{-1} K^{-1}. The Van't Hoff equation (i.e. the derivative of equation 15 assuming constant $\Delta_r H^\circ$ and $\Delta_r S^\circ$) can thus be regarded as a valid tool to extrapolate the stoichiometric saturation constant of LDH from 298 to higher temperatures (within the temperature range considered).

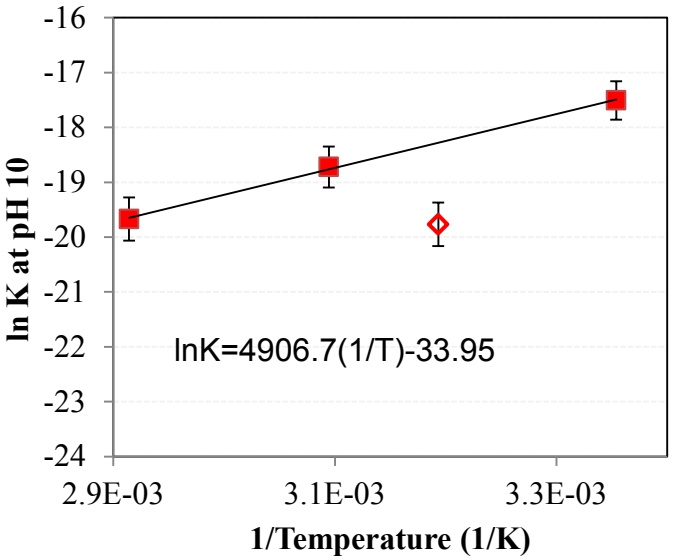

Fig 7: Stoichiometric saturation constants of Zr-LDH $Mg_{0.72}Al_{0.22}Zr_{0.025}(OH)_2Cl_{0.20}$ expressed as function of the inverse temperature. The experimental stoichiometric saturation constant at 313 K was excluded for a better fit. The estimated error on the ln K values is 0.05.

Table 5: Chemical composition of the aqueous solution after synthesis (equilibrium; pH = 10±0.05; total ionic strength ~0.19±0.01 M) and calculated stoichiometric saturation constant ln(K) of the Zr-LDH $Mg_{0.72}Al_{0.22}Zr_{0.025}(OH)_2Cl_{0.20}$.

Temperature [K]	Mg^{2+} [M]	Al^{3+} [M]	Zr^{4+} [M]	Cl^- [M]	ln(K) pH 10 eq. 2
298	3.3×10^{-03}	9.1×10^{-05}	1.0×10^{-05}	0.21	-17.5
313	1.6×10^{-03}	1.3×10^{-04}	1.3×10^{-05}	0.21	-19.8
323	5.4×10^{-04}	1.4×10^{-04}	1.3×10^{-05}	0.21	-18.7
343	2.3×10^{-04}	5.6×10^{-05}	3.8×10^{-06}	0.21	-19.7

It is worth to point out that the aqueous compositions at equilibrium with Zr-LDH reported in Table 5 are slightly oversaturated with respect to brucite, baddeleyite and gibbsite. This could suggest that a mixture of these phases of equivalent composition to Zr-LDH may represent the most stable phase assemblage in this system, while the absence of these phases and the

crystallization of LDH observed in the experiment could be attributed to kinetic factors. Indeed, kinetic difficulties of attaining the equilibrium have been previously reported for zirconia when the equilibrium was approached from oversaturation (Curti & Degueldre 2002). The crucial question we are trying to address here is whether the LDH is indeed stable with respect to the mechanical mixture of brucite, baddeleyite and gibbsite. To answer this question, the Gibbs energy formation of Zr-LDH should be estimated with the best possible precision. This estimation is discussed in sections 3.3, 3.4 and 3.5.

3.3 Gibbs free energy of formation from solution data

The Gibbs free energies of the synthesized Zr-containing LDH solids computed for different temperatures using GEM selector are presented in Table 6.The calculated Gibbs free energy of formation of the Zr-LDH $Mg_{0.72}Al_{0.22}Zr_{0.025}(OH)_2Cl_{0.20}*0.69H_2O$ varies between -1046±13 kJ mol^{-1} (298 K) and -1051±13 kJ mol^{-1} (343 K). The variation of the Gibbs free energy of formation, which relates to the stability of the LDH phase, is constant within the temperature range from 300 to 350 K. Generally, the Gibbs free energy of formation calculated from sum the chemical potentials depend on the temperature of the system; this effect is however minor for the considered temperature range. The Gibbs free energy is more strongly affected by the chemical composition of the solid which in our case is the same at all temperatures.

3.4 Gibbs energy of formation from calorimetric data

3.4.1 Enthalpies of Formation

The standard enthalpies of formation of the synthesized LDHs (ΔH_f°) were calculated from the heat effect associated with the dissolution of $Mg_{0.72}Al_{0.22}Zr_{0.025}(OH)_2Cl_{0.20}*0.69H_2O$ in 1M HCl acid (ΔH_{diss}/HCl) and in 1M HNO_3 (ΔH_{diss}/ HNO_3), respectively, at 298K.

The calorimetric measurements on the various LDH samples as well as on the metal chlorides and hydroxides were performed at least 3 times. Both methods yielded consistent results for ΔH_{diss} and ΔH_f^0.of the Zr-LDH. The enthalpies of dissolution of the Zr-LDH and the metal chlorides/ hydroxides as well as the standard enthalpy of formation of the Zr-LDH are reported in Table 7. The enthalpy of formation ΔH_f° of the Zr-LDH obtained by the two different methods is -1181±5 kJmol^{-1}.

Tables 6: Calculated Gibbs free energy of formation of the Zr-LDH $Mg_{0.72}Al_{0.22}Zr_{0.025}(OH)_2Cl_{0.20}$*0.69$H_2O$ with and without water as function of temperature. Errors were calculated using error propagation methods.

Temperature [K]	**Δ_fG GEMS [kJmol^{-1}] LDH (water free)**	**Δ_fG GEMS [kJmol^{-1}] LDH*0.69H_20**
298	-882.1±8.8	-1045.7±12.9
313	-881.5±8.9	-1045.9±13.0
323	-882.5±8.9	-1047.4±13.1
343	-885.1±9.0	-1051.1±13.2

Table 7: Measured enthalpies of dissolution ΔH_{diss} of the Zr-LDH $Mg_{0.72}Al_{0.22}Zr_{0.025}(OH)_2Cl_{0.20}$*0.69$H_2O$ and metal chlorides/hydroxides and derived enthalpy of formation of the Zr-LDH ΔH_f° (LDH).

Method 1: Dissolution in 1 M HCl	Method 2: Dissolution in 1 M HNO_3
ΔH_{diss}(LDH/HCl) = -85.8±1.0 kJmol^{-1}	ΔH_{diss}(LDH/HNO_3) = -83.9±0.9 kJmol^{-1} ΔH_{diss} ($Mg(OH)_2$) = ΔH1 = -105.7±3.0 kJmol^{-1} ΔH_{diss} ($MgCl_2$).6H_2O) = ΔH2 = -11.6±1.3 kJmol^{-1} ΔH_{diss} ($AlCl_3$.6H_2O) = ΔH3 = -47.1±2.0 kJmol^{-1} ΔH_{diss} ($ZrOCl_2$.8H_2O) = ΔH4 = -8.2±1.1 kJmol^{-1}
ΔH_f^0(LDH) = -1179±1 kJmol^{-1} (eq. 5)	ΔH_f^0(LDH) = -1182±4 kJmol^{-1} (eq. 13 & eq. 14)

The negative measured enthalpy of dissolution of the Zr-LDH in acidic media points to a strongly exothermic dissolution reaction and therefore indicates that a temperature increase is most likely to decrease the solubility of LDH (Le Chatelier's Principle). This is in good agreement with the observed effect of temperature on the solubility of the Zr-LDH reported in section 3.2.

3.4.2 Heat capacities and entropy

Heat capacity data measured for the Zr-LDH $Mg_{0.72}Al_{0.22}Zr_{0.025}(OH)_2Cl_{0.20}*0.69H_2O$, are plotted in Fig. 8. Heat capacities obtained for the series 2 samples were discarded, as the presence of an unknown amount of an amorphous impurity phase prevented a quantitative evaluation. The heat capacity values measured upon cooling differed significantly from the values measured upon heating at temperatures above 290 K. These differences are due to the loss of surface water and possibly also interlayer water at temperatures above 290 K, as observed in the TG-DSC measurements (Fig. 6). The PPMS measurements are conducted in vacuum, which will influence the release temperatures of adsorbed and incorporated water with respect to measurements at atmospheric pressure. Therefore, the data acquired up to 290 K were used and heat capacity values at higher temperature were extrapolated up to 300 K.

To simplify the derivation of thermodynamic functions, the heat capacity C_p was interpolated by a tenth degree polynomial between 2 K and 50 K and another tenth degree polynomial between 50 K and 290 K, where the latter then was used for an extrapolation to 300 K. The interpolated heat capacity is plotted in Fig. 8 as a solid line. The heat capacity of the Zr-LDH was evaluated to be 102 $kJmol^{-1}$ at 298 K.

When no electronic degrees of freedom are present, the third-law entropy of a solid S°, is given as the sum of the lattice and configurational contributions, $S^\circ = S^{\circ(cal)} + S^{\circ(conf)}$, with $S^{\circ(cal)}$ the lattice entropy of the solid and $S^{\circ(conf)}$, the configurational entropy.

The lattice entropy (or more appropriately, the vibrational entropy) of the synthesized LDH, for which no phase transition is observed, is determined as follows:

$$S^{\circ(cal)} = \int_0^T \frac{C_p}{T} dT \qquad (16)$$

where C_p is the heat capacity

The lattice entropy was evaluated to be 83.9 $Jmol^{-1}K^{-1}$ at 298.15 K.

The configurational entropy is associated with disorder of the cations in the octahedral layer and anions in interlayer crystallographic sites.

Assuming random (i.e. independent) substitution of Mg, Zr and Al in the brucite layer (complete disorder), the ideal configurational entropy for the brucite layer is given as (Allada et al. 2006):

$$S_{brucite}^{\circ(conf)} = -Rq[x_1 \ln x_1 + y_1 ln y_1 + z_1 ln z_1] \quad (17)$$

where $x_1=x/q$, $y_1=y/q$ and $z_1=z/q$ are the mole fractions of Mg, Al and Zr, in respectively, $q=x+y+z$ and R is the gas constant [8.314 $Jmol^{-1}K^{-1}$].The configurational entropy of the brucite layer of the Zr-LDH with x=0.72, y=0.22 and z=0.025 is therefore determined to be ~5.4 $Jmol^{-1}K^{-1}$

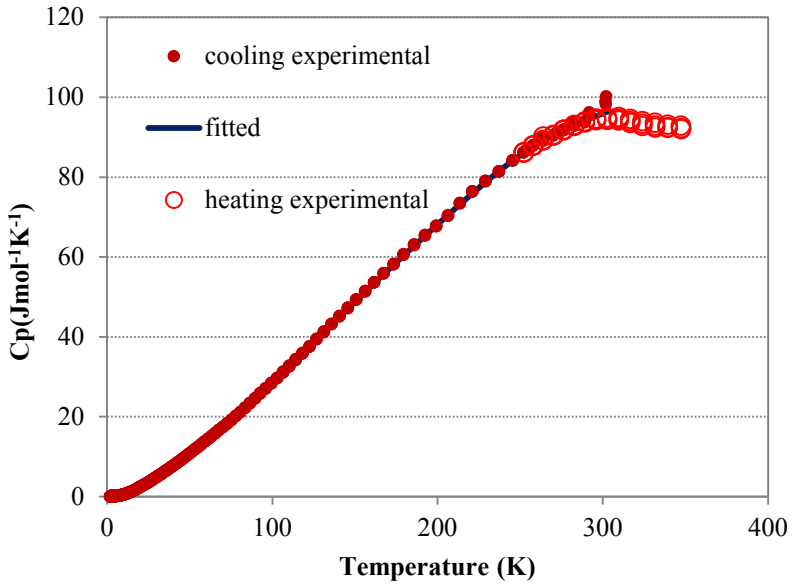

Fig. 8: Molar heat capacity of $Mg_{0.72}Al_{0.22}Zr_{0.025}(OH)_2Cl_{0.20}*0.69H_2O$. Data shown by open circles represent data obtained on heating, where a loss of adsorbed or incorporated water leads

to a change of the sample mass. These data were not used in the derivation of the thermodynamic properties.

The configurational entropy of the interlayer is calculated based on the number of vacant sites, anionic sites and H_2O sites, considering that H_2O takes an ice like structure in the interlayer (Van der Pol et al., 1994). Assuming a close packing of Cl^-, the fraction of vacant sites, *v*, is calculated as:

$$v = 1 - nCl^- - mH_2O \qquad (18)$$

where *n=0.20* and *m=0.69* are the mole fractions of Cl^- and H_2O respectively.

The ideal configurational entropy for the interlayer is given as:

$$S^{\circ(conf)}_{interlayer} = -R[v \ln v + mH_2Oln(mH_2O) + nCl^- \ln(nCl^-)] \qquad (19)$$

and is evaluated at ~6.8 $Jmol^{-1}K^{-1}$.

The total configurational entropy of the Zr-LDH is therefore ~12.2 $Jmol^{-1}K^{-1}$, which at 298.15 K translates to a contribution of -3.8 $kJmol^{-1}$ to the standard Gibbs free energy. It is important to note that the evaluation of the configurational entropy using the procedure described above, considers neither the positional disorder of water molecules, which could increase the entropy of the LDH, nor any effects of short range order (SRO), which could decrease this value. The possible error in the calculated configurational entropy due to these effects is estimated here as follows. The SRO within the brucite sheet is likely to be of avoidance type, meaning that the highly charged cations, i.e. Zr and Al would likely avoid the occupation of neighboring octahedral positions minimizing the Coulombic energy of their mutual repulsion. A similar type of SRO occurs, for example, in the tetrahedral layer of micas (Herrero and Sanz, 1991). The

555 configurational entropy of a solid solution with this type of SRO can be very roughly estimated
556 with the aid of the model of Kerrick and Darken (1975). This model emulates the SRO as the
557 long-range order by requesting the high-charge cations to occupy the sites of a certain sublattice,
558 while the other sublattice is assumed to be fully occupied by a low-charge cation. Here we
559 assume that Al and Zr atoms can freely mix with each other and with Mg only on one third of the
560 brucite layer sites, while the other two thirds of the sites are occupied only by Mg cations. In this
561 way the contacts between high-charge cations are completely avoided. Therefore, eq. 17 is
562 modified as follows

563 $$S_{brucite}^{(conf,sro)} = -R\frac{q}{3}[(3x_1 - 2)\ln(3x_1 - 2) + 3y_1 ln3y_1 + 3z_1 ln3z_1] \quad (20)$$

564 Using x, y and z equal to 0.72, 0.22 and 0.025 respectively, we obtain 2.1 $Jmol^{-1}$ K^{-1}. This implies
565 that the SRO of avoidance type can decrease the configurational entropy of the brucite layer by
566 as much as 60%. We assume that similar effects could also decrease the entropy of the anionic
567 layer. The rough estimate is that various types of SRO can decrease the total configurational
568 entropy by as much as 7 $Jmol^{-1}$ K^{-1}. On the other hand, the positional disorder of water molecules
569 would increase this value. Assuming that each molecule can occupy three equivalent positions
570 (only 3 and 6 positions would be consistent with the hexagonal symmetry), an increase in the
571 configurational entropy of water would be $Rm_{H2O}\ln 3$ = 6.3 $JK^{-1}mol^{-1}$for m_{H2O}= 0.69.
572 Consequently, the error in the configurational entropy is taken to be 6.5 $JK^{-1}mol^{-1}$(given by the
573 average of the computed positive and negative contributions) and the total configurational
574 entropy is taken to be 12±6.5 $Jmol^{-1}$ K^{-1}.

575 The standard entropy as composed of the vibrational and configurational contributions is thus
576 calculated as S° = 97±7 $Jmol^{-1}$ K^{-1}.

3.5 Thermodynamic data evaluation

The thermochemical data for the Zr-LDH $Mg_{0.72}Al_{0.22}Zr_{0.025}(OH)_2Cl_{0.20}*0.69H_2O$ derived in this work are summarized in Table 8.

Table 8: Summary of standard thermodynamic properties of the Zr-LDH $Mg_{0.72}Al_{0.22}Zr_{0.025}(OH)_2Cl_{0.20}*0.69H_2O$

$Mg_{0.72}Al_{0.22}Zr_{0.025}(OH)_2.0.69H_2O$	ΔH°_f [kJmol-1]	S° [$Jmol^{-1}K^{-1}$]	S°_f [$Jmol^{-1}K^{-1}$]	C_p 298.15 K [$Jmol^{-1}K^{-1}$]	G°_f [$kJmol^{-1}$]
Calorimetry	-1181±5	97±7	-453.8	102	-1046±7
Solubility (GEM approach)					-1046±13

The G°_f derived from calorimetric measurements was -1046 ±7 $kJmol^{-1}$. Using the co-precipitation experiment data, the standard Gibbs energy of formation of the synthesized solids G°_f was calculated using the Gibbs Energy Minimization approach (GEM approach). The value based on solubility data -1046±13 $kJmol^{-1}$ is in perfect agreement with the calorimetric data. Therefore, the Gibbs energy minimization approach can be seen as a valid tool for the evaluation of the thermodynamic data. The calculated Gibbs free energy of formation is in the same range of values as those calculated by Rozov et al., 2015 (~-872 $kJmol^{-1}$ for a water free Zr-LDH with Zr/(Zr+Al) ratio of 0.1) against -882±10 $kJmol^{-1}$ in our study. The differences can be explained by the slight variation in the stoichiometry of the solids.

The comparison with previously published thermodynamic data for the LDH is generally hampered due to the rather different compositions studied previously. Here, the thermodynamic properties of Zr-LDH with Cl as interlayer anion have been determined experimentally for the first time. However, the thermodynamic data derived in this work are generally comparable to the experimental measurements on CO_3^{2-}-bearing LDH (Allada et al. 2005b, 2006). It is

596 important to note that the authors used different methods involving high-temperature oxide-melt
597 solution calorimetry and low temperature adiabatic calorimeter for the measurement of enthalpy
598 and entropy respectively. Our experimental approach for the determination of the
599 thermodynamic properties determination is different but our results are consistent with values
600 reported for other LDH compounds.

601 Using the thermodynamic data (G°_{f}) at room temperature, the Gibbs free energy of the
602 dissolution reaction in acidic medium can be evaluated at 298 K and extrapolated to higher
603 temperatures using the Van't Hoff equation. The dissolution of Zr-LDH synthesized here can be
604 written as

605 $$Mg_{0.72}Al_{0.22}Zr_{0.025}(OH)_2Cl_{0.21} * 0.69H_2O + 2H^+ = 0.72Mg^{2+} + 0.22Al^{3+} + 0.025Zr^{4+} +$$
606 $$0.21Cl^- + 2.69H_2O \qquad (21)$$

607 The enthalpy of this reaction, ΔH_r, was previously measured in the calorimeter at -85.58 kJmol^{-1}
608 (dissolution in HCl). The entropy of reaction ΔS_r is given as $(\Delta H_r - \Delta G_r)\times(1/T)$ at -62 Jmol^{-1}.
609 Van't Hoff rewrites as:

610 $$lnk_r(T) = \left(\frac{85.7\times10^3}{R}\right)\frac{1}{T} + \frac{-62}{R} \qquad (22)$$

611 The log k_r and ΔG_r values of this reaction are provided in table 9 as function of temperature.

612 **Table 9**: Thermodynamic data (log k and ΔG_r°) of the dissolution of
613 $Mg_{0.72}Al_{0.22}Zr_{0.025}(OH)_2Cl_{0.20}*0.69H_2O$ in acidic medium.

Temperature [K]	ΔG_r [kJmol^{-1}] calculated	log k calculated
298	-67.1	11.8
313	-66.2	11.0
323	-65.6	10.6
343	-64.3	9.8

614

Based on the composition of the supernatant after synthesis (Table 5), the metastability of Zr-LDH with respect to a mechanical mixture of brucite, gibbsite and baddeleyite cannot be ruled out. To clarify this issue, the Gibbs energy of formation of the Zr –LDH is compared to the sum of the Gibbs energies of formation of these phases. The calorimetric $G°_f$ ($Mg_{0.72}Al_{0.22}Zr_{0.025}(OH)_2Cl_{0.20}\cdot 0.69H_2O$) is -1046±7 kJmol^{-1} while $\sum(0.62G_f^0(Mg(OH)_2) + +0.22G_f^0(Al(OH)_3) + 0.025G_f^0(ZrO_2) + 0.1G_f^0(MgCl_2) + 0.74G_f^0(H_2O))$ is -1030 kJmol^{-1}, which indicates that Zr-LDH is a more stable phase than the mechanical mixture of brucite, gibbsite and baddeleyite. However under our experimental conditions, it is unlikely that $MgCl_2$ (a highly soluble salt) will precipitate. The newly formed Zr-LDH can react as follows:

$$Mg_{0.72}Al_{0.22}Zr_{0.025}(OH)_2Cl_{0.20}.H_2O_{(s)} \rightarrow 0.62Mg(OH)_{2(s)} + 0.22Al(OH)_{3(s)} + 0.025ZrO_{2(S)} + 0.2Cl^-_{(aq)} + 0.1Mg^{2+}_{(aq)} + 0.74H_2O_{(l)} \quad (23)$$

The associated Gibbs free energy of reaction (G_r) and equilibrium constant (log K) are evaluated at -3 kJmol^{-1} and 0.512 respectively. Using the concentration of Mg^{2+} and Cl^- reported in Table 5, the ionic activity product (reaction 23) at the end of the experiment is equal to -0.384 which leads to a supersaturation index is of -0.896. This implies that the newly Zr-LDH will dissolve according to equation 23 to reach equilibrium. Therefore, it is most likely that the synthesized Zr-LDH is a metasble phase and a further reaction to form more stables phases (brucite, gibbsite and baddeleyite) is kinetically hindered.

4. Summary and conclusions

The aim of this work was to synthesize, characterize and determine the thermodynamic properties of Zr-containing LDH. Zr-containing LDHs were prepared by a co-precipitation

636 method at constant pH of 10 at Zr/(Al+Zr) of 0.1 and 0.4 respectively at temperatures ranging
637 from 298 to 343 K. Based on the characterization of the LDH, it is inferred that Zr^{4+} can be
638 incorporated into the brucite-like layers for the lower Zr/(Al+Zr) ratio, but precipitates as a
639 segregated amorphous hydrous Zr-oxide at higher Zr mole fractions. The maximum Zr uptake in
640 Cl^- bearing Mg-Al-LDH was found to be approximately 5 mol % compared to the 10 mol % Zr
641 previously incorporated in CO_3^{2-} bearing LDH by Shen et al. (2011), suggesting that the
642 interlayer anions affect the incorporation of Zr into the LDH structure. The effect of temperature
643 on the final composition of the LDH was found to be marginal, leading generally to a Zr-LDH of
644 the composition $Mg_{0.72}Al_{0.22}Zr_{0.025}(OH)_2Cl_{0.20}$ for the Zr/(Al+Zr) ratio of 0.1. The stoichiometric
645 saturation constant of the Zr- LDH was determined as function of temperature, revealing a
646 decrease in the solubility with increasing temperature, a common behavior of alkali metal
647 hydroxides. The stoichiometric saturation constant at different temperatures satisfied the Van't
648 Hoff equation, suggesting that the Van't Hoff equation can be regarded as a valid tool to
649 extrapolate the standard stoichiometric saturation constant of Zr-LDH from 298 to higher
650 temperatures.

651 This work also sheds light into the thermodynamic properties of Zr-LDH, reporting for the first
652 time experimentally derived thermodynamic data for Zr-bearing LDH, considering the Zr-LDH
653 $Mg_{0.72}Al_{0.22}Zr_{0.025}(OH)_2Cl_{0.20}*0.69H_2O$. We combined a an approach based on solubility data
654 and an experimental approach to estimate the Gibbs Free Energy of the Zr-LDH phase based on
655 calorimetry. Our approach based on solubility data included GEMs for the estimation of ΔG°_f.
656 Dissolution calorimetry and PPMS were used to determine the enthalpy of formation ΔH°_f and
657 entropy of the S° of the LDH system respectively. The approach based on solubility data and the
658 experimental approach for the determination of ΔG°_f were in excellent agreement.

659 This work provides relevant thermodynamic properties and stoichiometric saturation constants
660 that can be used for geochemical modeling of LDH in the geosphere.

661

Acknowledgements

The research leading to these results has received funding from the BMBF collaborative research project ThermAc via grant 02NUK039D. We gratefully thank Dr Hilde Curtius for her scientific support for the synthesis of LDH. The authors are also indebted to Katharina Dahmen, Thomas Krieger, Steve Lange, Giuseppe Modolo and Konstantin Rozov for their technical support in the analytical work and useful discussions.

References:

Aimoz, L., Taviot-Guého, C., Churakov S.V., Dähn, R., Chukalina M., Curti, E., Bordet, P., Vespa, M., (2012) Order of cation and anion in iodide-containing hydrotalcite-like minerals. J. Chem. Phys.C 116, 5460-5475.

Aimoz, L., Wieland, E., Taviot-Guého, C., Dähn, R., Vespa, M., Churakov, S.V., (2012) Structural insight into iodide uptake by AFm phases. Environ. Sci. Technol. 46 3874-3881

Aimoz, L., Kulik, D.A., Wieland, E., Curti, E., Lothenbach, B., Mäder, U., (2013) Thermodynamics of AFm-(I_2, SO_4) solid solution and of its end-members in aqueous media. Appl. Geochem. 27, 2117-2129.

Abdeloulas, A., Crovisier, J.L., Lutze, W., Fritz, B., Mosser, A., Müller, R. (1994) Formation of hydrotalcite-like compounds during R7T7 nuclear waste glass and basaltic glass alteration. Clays Clay Miner. 42, 526-533.

Allada, R.K., Pless, J.D., Nenoff, T.M., Navrotsky, A.M. (2005a) Thermochemistry of hydrotalcite-like phases intercalated with CO_3^{2-}, NO_3^-, Cl^-, I^-, and ReO_4^-. Chem. Mater. 17, 2455-2459.

Allada, R.K., Navrotsky, A., Boerio-Goates, J., (2005b) Thermochemistry of hydrotalcite phases in the MgO-Al_2O_3-CO_2-H_2O system: a determination of enthalpy, entropy and free energy. Am. Mineral. 90, 329-335.

Allada, R.K., Peltier, E., Navrotsky, A., Casey, W.M., Johnson, C.A., Thompson Berbeco, H., Sparks, D.L. (2006) Calorimetric determination of the enthalpies of formation of hydrotalcite-like solids and their use in the geochemical modeling of metals in natural waters. Clays Clay Miner., 54, 409-417.

Allmann, R. (1970) Doppelschichtstrukturen mit brucitähnlichen Schichtionen $[Me(II)_{1-x}$ $Me(III)_x(OH)_2]^{x+}$. Chimia 24, 99-107.

Allmann, R., Jepsen, H.P. (1969) Die Struktur des Hydrotalkits. Neues Jahrbuch für Mineralogie, Monatshefte, 544-551.

Aramendia, M.A., Borau, V., Jimenez, U., Marinas, J.M., Ruiz, J.R., Urbano, F.J (2002): Comparative study of Mg/M(III) (M = Al, Ga, In) layered double hydroxides obtained by coprecipitation and the sol-gel method. J. Solid State Chem. 168, 156-161.

Boclair, J.W., Braterman, P.S. (1999) Layered Double Hydroxide stability. 1. Relative stabilities of Layered Double Hydroxides and their simple counterparts. Chem. Mater. 11, 298-302.

Boclair, J.W., Braterman, P.S., Jiang, J.P., Lou, S.W., Yarberry, F., (1999) Layered double hydroxide stability. 2. Formation of Cr(III)-containing layered double hydroxides directly from solution. Chem. Mater. 11, 303-307.

703 Brindley, G.W., Kikkawa, S., (1980) Thermal-Behavior of hydrotalcite and of anion-exchanged
704 forms of hydrotalcite. Clays Clay Miner. 28, 87-91.

705 Brown, P.L., Curti, E., Grambow, B. (2005) Chemical thermodynamics of zirconium. Elsevier,
706 Amsterdam, 512.

707 Carlino, S., (1997) The intercalation of carboxylic acids into layered double hydroxides: A
708 critical evaluation and review of the different methods. Solid State Ion. 98, 73-84.

709 Carrado, K.A., Kostapapas, A., Suib, S.L., (1988) Layered double hydroxides (LDHs). Solid
710 State Ion. 26, 77-86.

711 Carteret, C., Gregoire, B., Ruby, C., (2011) Tunable composition of Ni-II-Al-III and Ni-II-Fe-III
712 layered hydroxides within a wide range of layer charge. Solid State Sci. 13, 146-150.

713 Cavani, F., Trifiro, F., Vaccari, A. (1991) Hydrotalcite-type anionic clays: Preparation,
714 properties and applications. Catal. Today 11, 173-301.

715 Chadwick, M.B., Herman, M., Obložinský, P., Dunn, M:E:, Danon, Y., Kahler, A.C., Smith, D.L.,
716 Pritychenko, B., Arbanas, G., Arcilla, R., Brewer, R., Brown, D.A., Capote, R., Carlson, A.D., Cho,
717 Y.S., Derrien, H., Guber, K., Hale, G.M., Hoblit, S., Holloway, S., Johnson, T.D., Kawano, T.,
718 Kiedrowski, B.C., Kim, H., Kunieda, S., Larson, N.M., Leal, L., Lestone, J.P., Little, R.C.,
719 McCutchan, E.A., MacFarlane, R.E., MacInnes, M., Mattoon, C.M., McKnight, R.D., Mughabghab,
720 S.F., Nobre, G.P.A., Palmiotti, G., Palumbo, A., Pigni, M.T., Pronyaev, V.G., Sayer, R.O., Sonzogni,
721 A.A., Summers, N.C., Talou, P., Thompson, I.J., Trkov, A., Vogt, R.L., van der Marck, C., Wallner,
722 A., White, M.C., Wiarda, D., Young, P.G., (2011) ENDF/B-VII.1 Nuclear Data for Science and
723 Technology: Cross Sections, Covariances, Fission Product Yields and Decay Data. Nuclear Data
724 Sheets 112, 2887-2996.

725 Chauvenet, E., (1913) Sur les oxychlorures de zirconium. Ann. Chim. Phys. 28, 536.

726 Chibwe, K., Jones, W., (1989) Intercalation of organic and inorganic anions into layered double
727 hydroxides. J. Chem. Soc. Chem. Commun. 14, 926-927.

728 Coughlin, J. P., (1958) Heats of formation and hydration of anhydrous aluminum chloride. J.
729 Chem. Phys. 62, 419-421.

730 Curti, E., Degueldre, C (2002) Solubility and hydrolysis of Zr oxides: a review and supplemental
731 data. Radiochim. Acta 90, 801–804

732 Curtius, H., Paparigas, Z., Kaiser, G., (2008) Sorption of selenium on Mg-Al and Mg-Al-Eu
733 layered double hydroxides. Radiochim. Acta 96, 651-655.

734 Curtius, H., Kattilparampil, Z. (2005) Sorption of iodine on Mg-Al-layered double hydroxide.
735 Clay Miner. 40, 455-461.

Curtius, H., Ufer, K., Dardenne, K., (2009) Preparation and characterization of Zr-IV-containing Mg-Al-Cl layered double hydroxide. Radiochim. Acta 96, 423-428.

Curtius, H., Kaiser, G., Rozov, K., Neumann, A., Daedenne, K., Bosbach, D. (2013) Preparation and characterization of Fe-, Co- and Ni- containing MgAl-layered double hydroxides. Clays Clay Miner. 61, 424-439.

Ditmars, D., Ishihara, S., Chang, S., Bernstein, G., West, E. (1982). Enthalpy and heat capacity standard reference material: synthetic sapphire (α-Al_2O_3) from 10 to 2250 K. J Res Natl Bur Stand. 87, 159-163.

Drits, V.A., Bookin, A.S. (2001) Crystal structure and X-ray identification of Layered Double Hydroxides. Chapter 2 in: Rives, V. (ed.) Layered double hydroxides: Present and future, Nova Science Publishers, New York, 41-100.

Fernández, R., Cuevas, J., Mäder, U.K. (2010) Modeling experimental results of diffusion of alkaline solutions through a compacted bentonite barrier. Cem. Concr. Res. 40, 1255-1265.

Galwey A.K, Laverty G.M., (1989) The thermal decomposition of magnesium chloride dihydrate. Thermochim. Acta 138, 115-127.

Glasser, F.P. (1997) Fundamental aspects of cement solidification and stabilisation. J. Hazard. Mater. 52, 151-170.

Helgeson, H.C., Kirkham, D.H., Flowers, G.C., (1981) Theoretical prediction of the thermodynamic behavior of aqueous electrolytes at high pressures and temperatures: IV. calculation of activity coefficients, osmotic coefficients, and apparent molal and standard and relative partial molal properties to 600°C and 5 KB. Am. J. Sci. 281, 1249-1516.

Helgeson, H.C., Delany, J.M, Nesbitt, H.W., Bird, D.K., (1978). Summary and critique of the thermodynamic properties of Rock-Forming Minerals., Am. J. Sci. 278A, 229.

Herrero, C.P., Sanz, J., (1991) Short-range order of the Si, Al distribution in layer silicates, J. Phys. Chem. Solids 52(9), 1129-1135.

Ingram, L., Taylor, H.F.W. (1967) The crystal structure of sjögrenite and pyroaurite. Mineralog. Mag. 36, 465-479.

Intissar, M., Jumas, J. C., Besse, J. P., Leroux, F., (2003) Reinvestigation of the layered double hydroxide containing tetravalent cations: Unambiguous response provided by XAS and Mossbauer spectroscopies. Chem. Mater. 15, 4625-4632.

Johnson, C.A., Glasser, F.P., (2003) Hydrotalcite-like minerals ($M_2Al(OH)_6(CO_3)_{0.5}.xH_2O$, where M = Mg, Zn, Co, Ni) in the environment: synthesis, characterization and thermodynamic stability. Clays Clay Miner., 51(1), 1-8.

769 Johnson, J.W., Oelkers, E.H., Helgeson, H.C., (1992) SUPCRT92: A software package for
770 calculating the standard molal thermodynamic properties of minerals, gases, aqueous species,
771 and reactions from 1 to 5000 bar and 0 to 1000 °C. Comput. Geosci., 18(7), 899-947.

772 Kerrick, D.M., Darken, L.S, (1975) Statistical thermodynamic models for ideal oxide and silicate
773 solid-solutions, with application to plagioclase. Geochim Cosmochim Acta, 39(10), 1431-1442.

774 Klinkenberg, M., Neumann, A., Curtius, H., Kaiser, G., Bosbach. D. (2014) Research reactor
775 fuel element corrosion under repository relevant conditions: separation, identification, and
776 quantification of secondary alteration phases of UAl_x-Al in $MgCl_2$-rich brine. Radiochim. Acta
777 102, 311-324.

778 Kulik, D.A., Wagner, T., Dmytrieva, S.V., Kosakowski, G., Hingerl, F.F., Chudnenko, K.V.,
779 Berner, U.R., (2013) GEM-Selektor geochemical modeling package: revised algorithm and
780 GEMS3K numerical kernel for coupled simulation codes. Comput. Geosci. 17: 1-24.

781 Lashley, J.C; Hundley, M.F; Migliori, A; Sarrao, J.L., Pagliuso, P.G., Darling, T.W., Jaime, M.,
782 Cooley, J.C., Hults, W.L., Morales, L., Thoma, D.J., Smith, J.L., Boerio-Goates, J., Woodfield,
783 B.F., (2003) Critical examination of heat capacity measurements made on a Quantum Design
784 physical property measurement system. Cryogenics, 43(6), 369-378.

785 Lydersen, E., (1990) The solubility and hydrolysis of aqueous aluminium hydroxides in dilute
786 fresh waters at different temperatures. Hydrol. Res., 21 (3) 195-204.

787 Mills, S.J., Christy, A.G., Génin. J.M.R., Kameda, T, Colombo, F. (2012) Nomenclature of the
788 hydrotalcite supergroup: natural layered double hydroxides. Mineralog. Mag. 76, 1289-1336.

789 Neumann, A., Klinkenberg, M., Curtius, H. (2016) Corrosion of non-irradiated UAlx–Al fuel in
790 the presence of clay pore solution: a quantitative XRD secondary phase analysis applying the
791 DDM method. Radiochim. Acta. 105, 85-94.

792 Miyata, S., Kumura, T., (1973) Synthesis of new hydrotalcite-like compounds and their
793 physicochemical properties. Chem. Lett. 843-848.

794 Prieto, M., (2009) Thermodynamics of solid solution-aqueous solution systems. Rev. Mineral.
795 Geochem. 70, 47-85.

796 Refait, P., Genin, J.-M.R., (1993) The oxidation of ferrous hydroxide in chloride-containing aqueous
797 media and Pourbaix diagrams of green rust one. Corros Sci. 34, 797-819.

798 Rives, V. (2001): Layered double hydroxides: Present and future, Nova Science Publishers, New
799 York, 439.

800 Rives, V. (2002) Characterization of layered double hydroxides and their decomposition
801 products. Mater. Chem. Phys. 75, 19–25.

802 Rozov, K., Berner, U., Taviot-Gueho, C., Leroux, F., Renaudin, G., Kulik, D., Diamond, L.W.,
803 (2010) Synthesis and characterization of the LDH hydrotalcite-pyroaurite solid solution series.
804 Cem. Concr. Res. 40, 1248-1254.

805 Rozov, K.B., Berner, U., Kulik, D.A., Diamond, L.W., (2011) Solubility and thermodynamic
806 properties of carbonate-bearing hydrotalcite-pyroaurite solid solutions with a 3:1 Mg/(Al+Fe)
807 mole ratio. Clays Clay Miner. 59, 215-232.

808 Rozov, K., Curtius, H., Neumann, A., Bosbach, D., (2013) Synthesis, characterization and
809 stability properties of Cl-bearing hydrotalcite-pyroaurite solids. Radiochim. Acta 101, 101-109.

810 Rozov, K., Curtius, H., Bosbach., H., (2015) Preparation, characterization and thermodynamic
811 properties of Zr-containing Cl-bearing layered double hydroxides (LDHs). Radiochim. Acta 103,
812 369-378.

813 Scheidegger, A.M., Lamble, G.M., Sparks, D.L. (1997) Spectroscopic evidence for the formation
814 of mixed-cation hydroxide phases upon metal sorption on clays and aluminum oxides. J. Colloid
815 Interface Sci. 186, 118-128.

816 Shen, Y., Liu, D., Fan, L., Li, S., Gao, L., (2011) Simultaneous incorporation of palladium and
817 zirconium ions in Mg-Al layered double hydroxides by co-precipitation. Appl Clay Sci. 54, 179-
818 183.

819 Shock, E.L., Helgeson, H.C., Sverjensky, D.A., (1989) Calculation of the thermodynamic and
820 properties of aqueous species at high pressures temperatures: Standard partial molal properties
821 inorganic neutral species. Geochim. Cosmochim. Acta 53, 2157-2183.

822 Shock, E.L, Sassani, D.C., Willis M., Sverjensky, D.A., (1997) Inorganic species in geologic
823 fluids: Correlations among standard molal thermodynamic properties of aqueous ions and
824 hydroxide complexes. Geochim. Cosmochim. Acta 61(5), 907-950.

825 Shomate, C.H., Huffmann E.H., (1943) Heats of formation of MgO, $MgCl_2$, $MgCl_2 \cdot 4H_2O$ and
826 $MgCl_2 \cdot 6H_2O$. J. Am. Chem. Soc. 65, 1623-1629.

827 Skovbjerg, L.L., Christiansen, B.C., Nedel, S., Dideriksen, K., Stipp, S.L.S. (2010) The role of
828 green rust in the migration of radionuclides: An overview of processes that can control mobility
829 of radioactive elements in the environment using as examples Np, Se and Cr. Radiochim. Acta
830 98, 607-612.

831 Taylor, H.F.W. (1973) Crystal structures of some double hydroxide minerals. Mineralog. Mag.
832 39, 377-389.

833 Taylor, H.F.W. (1997) Cement chemistry (2nd edition). Thomas Telford Publishing, London, 459
834 S.

Thoenen, T., Hummel, W., Berner, U., Curti, E., (2014) The PSI/Nagra chemical thermodynamic database 12/07. NAGRA Arbeitsbericht NAB 14-49.

Van der Pol, A., Mojet, B.L, Vandeven, E., Deber, E. (1994) Ordering of intercalated water and carbonate anions in Hydrotalcite- Ann NMR study. J. Phys. Chem., 98, 4050-4054.

Velu, S., Sabde, D. P., Shah, N., Sivasanker, S., (1998) New hydrotalcite-like anionic clays containing Zr^{4+} in the layers: Synthesis and physicochemical properties. Chem. Mater. 10, 3451–3458.

Wagner, T., Kulik, D.A., Hingerl, F.F., Dmytrievava, S.V., (2012) GEM-Selektor geochemical modeling package: TSolMod library and data interface for multicomponent phase models. Can. Mineral. 50, 1173-1195.

Wersin, P., Johnson, L.H., Schwyn, B., Berner, U., Curti, E., (2003) Redox conditions in the near field of a repository for SF/HLW and ILW in Opalinus Clay. Nagra NTB 02-13

Wersin, P., Birgersson, M. (2014) Reactive transport modelling of iron–bentonite interaction within the KBS-3H disposal concept: the Olkiluoto site as a case study. Geol Soc Spec Publ. 400, 237-250.